

A C^0 LINEAR FINITE ELEMENT METHOD FOR SIXTH ORDER ELLIPTIC EQUATIONS

HAILONG GUO*, ZHIMIN ZHANG [†], AND QINGSONG ZOU[‡]

Abstract. In this paper, we develop a straightforward C^0 linear finite element method for sixth-order elliptic equations. The basic idea is to use gradient recovery techniques to generate higher-order numerical derivatives from a C^0 linear finite element function. Both theoretical analysis and numerical experiments show that the proposed method has the optimal convergence rate under the energy norm. The method avoids complicated construction of conforming C^2 finite element basis or nonconforming penalty terms and has a low computational cost.

AMS subject classifications. Primary 65N30; Secondary 45N08

Key words. Sixth-order equation, Gradient recovery, Linear finite element.

1. Introduction. Partial differential equations (PDEs) with order higher than 2 have been widely used to describe different physical laws in material sciences [14, 15, 29, 30, 39], elastic mechanics [42], quantum mechanics [24], plasma physics [10, 11, 22], differential geometry [16, 41], and other areas of science and engineering. Comparing with the second-order PDEs, higher order PDEs are much less studied, including some fundamental theoretical issues such as existence, uniqueness, and regularity of solutions.

Numerical simulation becomes an important tool to study high order PDEs, and yet the design of efficient and reliable numerical methods is very challenging. As usual, the finite element method (FEM) plays a critical role in the numerical simulation. Both conforming and nonconforming methods have been applied to solve high order PDEs in the literature. Usually, a conforming method requires higher regularity of the approximating functions (e.g. C^1 functions for a fourth-order PDE and C^2 for a sixth-order PDE), while a nonconforming method avoids the construction of higher regularity finite elements by adding some specially designed penalty terms to the scheme. The complicated construction of high regularity finite elements (for conforming methods) or penalty terms (for nonconforming methods) makes these two FEMs hard to be implemented and significantly increases computational cost. Moreover, the analysis of the aforementioned FEMs is often very complicated.

In this work, we present a systematic and simple numerical approach to treat high-order PDEs and shed some light on theoretical analysis for this new method. To be more precise, we will develop a gradient recovery technique based C^0 linear finite

* Department of Mathematics, University of California Santa Barbara, CA, 93106 (hlguo@math.ucsb.edu).

[†]Beijing Computational Science Research Center, Beijing 100094 and Department of Mathematics, Wayne State University, Detroit, MI 48202 (zzhang@math.wayne.edu). The research of this author was supported in part by the National Natural Science Foundation of China under grants 11471031, 91430216, U1530401, and the U.S. National Science Foundation through grant DMS-1419040.

[‡]Corresponding author. School of Data and Computers and Guangdong Province Key Laboratory of Computational Science, Sun Yat-sen University, Guangzhou 510275 (mcszqs@mail.sysu.edu.cn). This author was partially supported by the National Natural Science Foundation of China through grants 11571384 and 11428103, by Guangdong Provincial Natural Science Foundation of China through grant 2014A030313179, and by the Fundamental Research Funds for the Central Universities through the grant 16lgjc80.

element method for the following sixth-order equation

$$-\Delta^3 u = f \quad \text{in } \Omega \quad (1.1)$$

$$u = \partial_{\mathbf{n}} u = \partial_{\mathbf{nn}}^2 u = 0 \quad \text{on } \partial\Omega, \quad (1.2)$$

where $\Omega \subset \mathbb{R}^2$ is an open bounded domain, $f \in L^2(\Omega)$, \mathbf{n} is the outward unit normal of the boundary $\partial\Omega$. The sixth order derivative is defined as

$$\Delta^3 u = \Delta(\Delta(\Delta u)) = \sum_{i,j,k=1}^2 \frac{\partial^6 u}{\partial x_i^2 \partial x_j^2 \partial x_k^2}$$

and the directional derivatives are $\partial_{\mathbf{n}} u = \nabla u \cdot \mathbf{n}$, $\partial_{\mathbf{nn}}^2 u = \mathbf{n}^T D^2 u \cdot \mathbf{n}$. The (weak) solution of (1.1)-(1.2) is a function $u \in H_0^3(\Omega)$ satisfying

$$a(u, v) = (f, v), \forall v \in H_0^3(\Omega), \quad (1.3)$$

where the third order derivative tensor is given by $D^3 v = \frac{\partial^3 v}{\partial x_i \partial x_j \partial x_k}$ and the bilinear form is

$$a(v, w) = \int_{\Omega} D^3 v : D^3 w, \quad \forall v, w \in H^3(\Omega).$$

Here the Frobenius product “:” for two tensors $B_1 = (b_{ijk}^1)$, $B_2 = (b_{ijk}^2)$ is defined as

$$B_1 : B_2 = \sum_{i,j,k=1}^2 b_{ijk}^1 b_{ijk}^2.$$

Note that the sixth-order elliptic boundary value problem (1.1) arises from many mathematical models including differential geometry ([16, 41]), the thin-film equations [9], and the phase field crystal model [8, 18, 40]. For simplicity, we choose the homogeneous Dirichlet boundary conditions. The basic principle can be applied to other boundary conditions as well.

Let us illustrate the basic idea of the construction of our novel method. Note that the bilinear form $a(\cdot, \cdot)$ involves the third derivative of the discrete solution, which is impossible to obtain from a direct calculation of C^0 linear element whose gradient is piecewise constant (w.r.t the underlying mesh) and discontinuous across each element. To overcome this difficulty, we use the gradient recovery operator G_h to “lift” discontinuous piecewise constant Dv_h to continuous piecewise linear function $G_h v_h$, see [?, 2–5, 7, 20, 45, 47] for the details of different recovery operators. In other words, we use the special *difference operator* DG_h^2 to discretize the third order differential operator D^3 . Our algorithm is then designed by applying this special *difference operator* to the standard Ritz-Galerkin method.

From the above construction, our method has some obvious advantages. First, the fact that the recovery operator G_h can be defined on a general unstructured grid implies that the method is valid for problems on arbitrary domains and meshes. Second, our method only has function value unknowns on nodal points instead of both function value and derivative unknowns, its computational complexity is much lower than existing conforming and non-conforming methods in the literature.

Naturally, one may question on the consistency, stability, and convergence of the proposed method, which require some more in-depth mathematical analysis. Let us

begin with a discussion of consistency. As indicated in [45] (resp. [25]), for reasonably regular meshes, $G_h u_I$ (resp. $G_h^2 u_I$) is a second-order finite difference scheme of the gradient Du (resp. D^2u), if u is sufficiently smooth. Here u_I is the interpolation of u in linear finite element space. As a consequence, $DG_h^2 u_I$ is a first-order approximation of D^3u , provided u is sufficiently smooth. However, for a discrete function v_h in the finite element space which is not smooth across the element edges, the error $\|Dv_h - G_h v_h\|_0$ is not a small quantity of the high order, sometimes it may not converge to zero at all. Fortunately, an error estimate in [17, 26] set up a consistency in a weak sense, see (3.6) and (3.7) for the details. This weak consistency property of the gradient recovery operator will play an important role in our error analysis.

Next we discuss stability, which in our case can be reduced to verification of the (uniform) coercivity of the bilinear form $(DG_h^2 \cdot, DG_h^2 \cdot)$ in the following sense

$$\|v_h\|_0 \lesssim \|DG_h^2 v_h\|_0, \quad (1.4)$$

for all v_h in the finite element space with suitable boundary conditions. Again, since the *discrete Poincaré inequality* (3.5) has been established in [26], the stability (1.4) is a direct consequence. Note that (1.4) implies that no additional penalty term is needed in order to guarantee the stability, and this fact makes our method very simple.

The convergence properties of our method depends heavily on the aforementioned consistency, stability, and the nice approximation properties of the recovery operator G_h . As usual, the analysis of the error between the exact and approximate solutions can be decomposed into the analysis of the approximation error and consistency error. Combining the weak consistency error estimates (3.6),(3.7) and approximation error estimates (3.2)-(3.4) leads to the optimal convergence rate ($= 1$) under the energy norm (H^3 norm). This convergence rate is observed numerically. Furthermore, we also notice a second-order convergence rate under both H^1 and L^2 norms. However, we are only able to prove a sub-optimal convergence rate $\frac{3}{2}$ under both the H^1 and L^2 norms at this moment. We would like to emphasize that our analysis here is straightforward and simpler than the analysis of traditional conforming and nonconforming methods applied to sixth-order PDEs.

The rest of the paper is organized as follows. We first present our algorithm in Section 2. Several numerical examples are provided in Section 3 to illustrate the efficiency and convergence rates of our algorithm. In Section 4, a rigorous mathematical analysis of our algorithm is given. Finally, some concluding remarks are presented in the final section.

2. A recovery based C^0 linear FEM. In this section, we discretize the variational equation (1.3) in the standard C^0 linear finite element space.

Let \mathcal{T}_h be a *triangulation* of Ω with mesh-size h . We denote by \mathcal{N}_h and \mathcal{E}_h the set of vertices and edges of \mathcal{T}_h , respectively. Let V_h be the standard \mathcal{P}_1 finite element space corresponding to \mathcal{T}_h . It is well-known that $V_h = \text{Span}\{\phi_p : p \in \mathcal{N}_h\}$ with ϕ_p a linear nodal basis corresponding to each vertex $p \in \mathcal{N}_h$. Let $G_h : V_h \rightarrow V_h \times V_h$ be a gradient recovery operator defined as below ([34, 47]). For each vertex $p \in \mathcal{N}_h$, we define a recovered derivative $(G_h v_h)(p)$ and let the whole recovered gradient function be

$$G_h v_h = \sum_{p \in \mathcal{N}_h} (G_h v_h)(p) \phi_p.$$

For all $v_h \in V_h$, we have $G_h v_h = (G_h^{x_1} v_h, G_h^{x_2} v_h) \in V_h \times V_h$. The corresponding

recovered Hessian matrix is defined as follows [25]:

$$G_h^2 v_h = \begin{pmatrix} G_h^{x_1} G_h^{x_1} v_h & G_h^{x_1} G_h^{x_2} v_h \\ G_h^{x_2} G_h^{x_1} v_h & G_h^{x_2} G_h^{x_2} v_h \end{pmatrix}.$$

The derivative of $G_h^2 v_h$ is a tensor with its component

$$(DG_h^2 v_h)_{ijk} = \partial_{x_i} G_h^{x_j} G_h^{x_k} v_h, \quad i, j, k = 1, 2.$$

For all $v_h, w_h \in V_h$, we define a *discrete* bilinear form

$$a_h(v_h, w_h) = \int_{\Omega} D(G_h^2 v_h) : D(G_h^2 w_h),$$

The gradient recovery linear element scheme for solving (1.1) reads as : Find $u_h \in V_h^0$ such that

$$a_h(u_h, v_h) = (f, v_h), \quad v_h \in V_h^0, \quad (2.1)$$

where the homogenous finite element space

$$V_h^0 = \{v_h \in V_h | v_h = G_h v_h \cdot \mathbf{n} = G_h v_h \cdot \mathbf{t} = \mathbf{n}^T G_h^2 v_h \mathbf{n} = 0 \text{ on } \partial\Omega\}.$$

Note that here we use an additional condition $G_h v_h \cdot \mathbf{t} = 0$ since the exact solution satisfies $\frac{\partial u}{\partial \mathbf{t}} = 0$ on $\partial\Omega$, where \mathbf{t} is the unit tangential vector on $\partial\Omega$.

REMARK 2.1. *For sixth order partial differential equation (1.1)-(1.2), all three boundary conditions are essential boundary conditions and we should incorporate such types boundary conditions into the discretized linear system instead of the weak form. For partial differential equation (1.1) with nonhomogeneous boundary conditions*

$$u|_{\partial\Omega} = g_D, \quad \partial_{\mathbf{n}} u|_{\partial\Omega} = g_N, \quad \partial_{\mathbf{nn}}^2 u|_{\partial\Omega} = g_R. \quad (2.2)$$

The variation form is to find $u_h \in V_h$ with $u_h|_{\partial\Omega} = g_D, \partial_{\mathbf{n}} u_h|_{\partial\Omega} = g_N, \partial_{\mathbf{nn}}^2 u_h|_{\partial\Omega} = g_R$ such that

$$a_h(u_h, v_h) = (f, v_h), \quad v_h \in V_h^0,$$

For numerical implement, there is no difference between homogeneous and nonhomogeneous boundary conditions. In the article, we suppose homogeneous boundary conditions only for simplifying numerical analysis.

REMARK 2.2. *The scheme (2.1) depends on the definition of $(G_h v_h)(p)$ at each vertex $p \in \mathcal{N}_h$. In the following, three popular definitions of $(G_h v_h)(p)$ are listed (c.f., [34, 47]).*

(a) *Weighted averaging (WA).* For each $p \in \mathcal{N}_h$, let the element patch $\omega_p = \cup\{\tau : p \in \bar{\tau}\}$ and define

$$(G_h v_h)(p) = \frac{1}{|\omega_p|} \int_{\omega_p} \nabla v_h(x_1, x_2) dx_1 dx_2. \quad (2.3)$$

(b) *Local L^2 -projection.* We seek two polynomials $P_l \in \mathcal{P}^1(\omega_p)$, ($l = 1, 2$), such that

$$\int_{\omega_p} [P_l(x_1, x_2) - \partial_{x_l} v(x_1, x_2)] Q(x_1, x_2) dx_1 dx_2 = 0, \quad \forall Q \in \mathcal{P}^1(\omega_p), l = 1, 2 \quad (2.4)$$

and we define

$$(G_h v_h)(p) = (P_1(p), P_2(p)).$$

Sometimes, the exact integral in (2.4) is replaced by its discrete counterpart so that the two polynomials $P_l, l = 1, 2$ satisfying the least square fitting equation (SPR)

$$\sum_{i=1}^m [P_l(x_1^i, x_2^i) - \partial_{x_i} v(x_1^i, x_2^i)] Q(x_1^i, x_2^i) = 0, \quad \forall Q \in \mathcal{P}^1(\omega_P), l = 1, 2, \quad (2.5)$$

where $(x_1^i, x_2^i), i = 1, \dots, m$ are m given points in ω_p .

(c) The polynomial preserving recovery (PPR). We seek a quadratic function $P \in \mathcal{P}^2(\omega_p)$, such that

$$\sum_{i=1}^m [P(x_1^i, x_2^i) - v(x_1^i, x_2^i)] Q(x_1^i, x_2^i) = 0, \quad \forall Q \in \mathcal{P}^2(\omega_P). \quad (2.6)$$

Then we can define $(G_h v_h)(p) = (\partial_{x_1} P(p), \partial_{x_2} P(p))$.

It is known that the above three definitions are equivalent on a mesh of uniform triangular pattern [45].

REMARK 2.3. Essentially, the operator G_h can be regarded as a difference operator defined on unstructured grids. This operator lifts discontinuous gradient generated from a C^0 -FEM to a continuous one, and thereby makes the further calculation of high order derivatives possible.

REMARK 2.4. The scheme (2.1) is very simple and straightforward. It avoids the complicated construction of conforming C^2 finite element basis (c.f., [28]) or the complicated construction of nonconforming penalty terms ([27]).

For $\mathcal{A} \subset \Omega$, let $V_h(\mathcal{A})$ denote the restrictions of functions in V_h to \mathcal{A} and let $V_h^{\text{comp}}(\mathcal{A})$ denote the set of those functions in $V_h(\mathcal{A})$ with compact support in the interior of \mathcal{A} [37]. Let $\Omega_0 \subset\subset \Omega_1 \subset\subset \Omega_2 \subset\subset \Omega$ be separated by $d \geq c_o h$ and ℓ be a direction, i.e., a unit vector in \mathbb{R}^2 . Let τ be a parameter, which will typically be a multiply of h . Let T_τ^ℓ denote translation by τ in the direction ℓ , i.e.,

$$T_\tau^\ell v(x) = v(x + \tau\ell), \quad (2.7)$$

and for an integer ν

$$T_{\nu\tau}^\ell v(x) = v(x + \nu\tau\ell). \quad (2.8)$$

Following the definition of [37], the finite element space V_h is called translation invariant by τ in the direction ℓ if

$$T_{\nu\tau}^\ell v \in V_h^{\text{comp}}(\Omega), \quad \forall v \in V_h^{\text{comp}}(\Omega_1), \quad (2.9)$$

for some integer ν with $|\nu| < M$. Equivalently, \mathcal{T}_h is called a translation invariant mesh. As illustrated in [25], uniform meshes of regular pattern, chevron pattern, cirsscross patter, and unionjack pattern are all translation invariant.

3. Analysis. The section is dedicated to a mathematical proof for the convergence properties.

To this end, we need some properties of G_h . For the polynomial preserving recovery operator G_h , there are the following boundedness property (see (2.11) in [34])

$$\|G_h v_h\|_0 \lesssim |v_h|_1, \quad v_h \in V_h \quad (3.1)$$

and the superconvergence approximation properties

$$\|\nabla u - G_h u_I\|_0 \lesssim h^2 |u|_{3,\infty}, \quad u \in W^{3,\infty}(\Omega). \quad (3.2)$$

Here u_I is the linear interpolation of u in V_h . In addition, we will utilize the following ultraconvergence approximation properties of Hessian recovery operator (see Theorem 3.5 in [25])

$$\|D^3 u - DG_h^2 u_I\|_0 \lesssim h |u|_{4,\infty}, \quad u \in W^{4,\infty}(\Omega), \quad (3.3)$$

$$\|D^2 u - G_h^2 u_I\|_0 \lesssim h^2 |u|_{4,\infty}, \quad u \in W^{4,\infty}(\Omega), \quad (3.4)$$

provided the mesh \mathcal{T}_h is translation invariant.

REMARK 3.1. *We would like to comment that the requirement \mathcal{T}_h translation invariant for proving approximation properties (3.3) and (3.4) only for theoretical purpose. In practical, our method can be applied to and shows optimal convergence on arbitrary unstructured mesh.*

To analyze the convergence of the scheme (2.1), we suppose that the \mathcal{T}_h is sufficient regular such that there holds the following discrete Poincaré inequality (cf., [26])

$$\|v_h\|_i \lesssim \|G_h v_h\|_i, \quad \forall v_h \in V_h^0, i = 0, 1 \quad (3.5)$$

and discrete *weak* approximation properties

$$\left| \int_{\Omega} \nabla v \cdot (G_h v_h - \nabla v_h) \right| \lesssim h \|v\|_2 |G_h v_h|_1, \quad \forall v \in H^2, \quad (3.6)$$

$$\left| \int_{\Omega} \nabla v \cdot (G_h v_h - \nabla v_h) \right| \lesssim h^2 \|v\|_3 |G_h v_h|_1, \quad \forall v \in H^3. \quad (3.7)$$

Note that both (3.5) and (3.6) have been discussed in the analysis of a recovery operator based linear finite element method for the biharmonic equation by Guo et al. in [26]. In their paper, a counter-example shows that the strong error $\|\nabla v_h - G_h v_h\|_0$ is not necessary of $\mathcal{O}(h)$ for all $v_h \in V_h$ (which means the weak estimate (3.6) might be the best estimate of the difference $\nabla v_h - G_h v_h$).

By (3.5), for all $v_h \in V_h^0$, we have

$$\|v_h\|_0 \lesssim \|G_h v_h\|_0 \lesssim \|G_h^2 v_h\|_0 \lesssim \|DG_h^2 v_h\|_0.$$

In other words, the semi-norm $\|DG_h^2 \cdot\|_0$ is a norm. Then by the Lax-Milgram theorem, the scheme (2.1) has a unique solution. Moreover, by (2.1),

$$\|DG_h^2 u_h\|_0^2 = a_h(u_h, u_h) = (f, u_h) \lesssim \|f\|_0 \|v_h\|_0.$$

Then

$$\|DG_h^2 u_h\|_0 \lesssim \|f\|_0 \quad (3.8)$$

which implies the stability of our scheme.

3.1. H^3 error estimate. **THEOREM 3.1.** *Let u_h be the solution of (2.1) and $u \in H^6$ the solution of (1.3). If the mesh \mathcal{T}_h is translation invariant, G_h is properly defined such that (3.1)-(3.7) hold, then*

$$\|DG_h^2(u_h - u_I)\|_0 \lesssim h \|u\|_6, \quad (3.9)$$

where u_I is the linear interpolation of u in V_h . Consequently,

$$\|D^3u - DG_h^2u_h\|_0 \lesssim h\|u\|_6. \quad (3.10)$$

Proof. Since a weak solution of (1.3) which has regularity $u \in H^6$ is also the strong solution satisfying (1.1) and u_h is a discrete solution satisfying (2.1), we have

$$a_h(u_h, v_h) = (f, v_h) = (-\Delta^3u, v_h), \forall v_h \in V_h^0.$$

Using the fact that $v_h \in V_h^0$, we have

$$(-\Delta^3u, v_h) = (-\nabla \cdot \nabla)(\Delta^2u, v_h) = (\nabla(\Delta^2u), \nabla v_h).$$

Therefore,

$$a_h(u_h, v_h) = I_1 + (\nabla(\Delta^2u), G_h v_h),$$

with

$$I_1 = (\nabla(\Delta^2u), \nabla v_h - G_h v_h). \quad (3.11)$$

Now we deal with the term $(\nabla(\Delta^2u), G_h v_h)$. Since $G_h v_h \cdot \mathbf{n} = G_h v_h \cdot \mathbf{t} = 0$ on the boundary $\partial\Omega$, we have that on $\partial\Omega$,

$$\frac{\partial \Delta u}{\partial \mathbf{n}} \cdot G_h v_h = \frac{\partial^2 \Delta u}{\partial \mathbf{n} \partial \mathbf{t}} (G_h v_h \cdot \mathbf{t}) + \frac{\partial^2 \Delta u}{\partial \mathbf{n}^2} (G_h v_h \cdot \mathbf{n}) = 0.$$

Then

$$\begin{aligned} (\nabla(\Delta^2u), G_h v_h) &= ((\nabla \cdot \nabla)(\Delta(\nabla u)), G_h v_h) \\ &= -(D^2(\Delta u), DG_h v_h) := - \int_{\Omega} D^2(\Delta u) : DG_h v_h. \end{aligned}$$

Consequently,

$$(\nabla(\Delta^2u), G_h v_h) = I_2 - (D^2(\Delta u), G_h^2 v_h),$$

with

$$I_2 = (D^2(\Delta u), G_h^2 v_h - DG_h v_h). \quad (3.12)$$

Finally, we deal with the term $-(D^2(\Delta u), G_h^2 v_h)$. Writing the gradient as

$$\nabla u = \frac{\partial u}{\partial \mathbf{n}} \mathbf{n} + \frac{\partial u}{\partial \mathbf{t}} \mathbf{t},$$

we have

$$D^2u = \frac{\partial^2 u}{\partial \mathbf{n}^2} \mathbf{n} \mathbf{n}^T + \frac{\partial^2 u}{\partial \mathbf{t}^2} \mathbf{t} \mathbf{t}^T + \frac{\partial^2 u}{\partial \mathbf{n} \partial \mathbf{t}} (\mathbf{n} \mathbf{t}^T + \mathbf{t} \mathbf{n}^T),$$

and consequently,

$$\frac{\partial D^2u}{\partial \mathbf{n}} = \frac{\partial^3 u}{\partial \mathbf{n}^3} \mathbf{n} \mathbf{n}^T + \frac{\partial^3 u}{\partial \mathbf{n} \partial \mathbf{t}^2} \mathbf{t} \mathbf{t}^T + \frac{\partial^3 u}{\partial \mathbf{n}^2 \partial \mathbf{t}} (\mathbf{n} \mathbf{t}^T + \mathbf{t} \mathbf{n}^T).$$

Noting that $u = \frac{\partial u}{\partial \mathbf{n}} = \frac{\partial^2 u}{\partial \mathbf{n}^2} = 0$ on $\partial\Omega$, we have

$$\frac{\partial^3 u}{\partial \mathbf{n} \partial \mathbf{t}^2} = \frac{\partial^3 u}{\partial \mathbf{n}^2 \partial \mathbf{t}} = 0 \text{ on } \Omega.$$

Therefore, on $\partial\Omega$,

$$\frac{\partial D^2 u}{\partial \mathbf{n}} : G_h^2 v_h = \frac{\partial^3 u}{\partial \mathbf{n}^3} \mathbf{n} \mathbf{n}^T : G_h^2 v_h = \frac{\partial^3 u}{\partial \mathbf{n}^3} \mathbf{n}^T G_h^2 v_h \mathbf{n} = 0,$$

where in the last equality, we used the fact that $\mathbf{n}^T G_h^2 v_h \mathbf{n} = 0$. By Green's formulas, we finally obtain

$$-(D^2(\Delta u), G_h^2 v_h) = -(\Delta(D^2 u), G_h^2 v_h) = (D^3 u, DG_h^2 v_h).$$

In summary, by letting

$$I_3 = (D^3 u - DG_h^2 u_I, DG_h^2 v_h),$$

we obtain

$$a_h(u_h - u_I, v_h) = I_1 + I_2 + I_3. \quad (3.13)$$

Next, we estimate I_i ($i = 1, 2, 3$) term by term. By (3.5) and (3.6), we have

$$|I_1| \lesssim h \|u\|_6 \|G_h v_h\|_1 \lesssim h \|u\|_6 \|DG_h^2 v_h\|_0.$$

Similarly, by (3.3),

$$|I_3| \lesssim h \|u\|_{4,\infty} \|DG_h^2 v_h\|_0 \lesssim h \|u\|_6 \|DG_h^2 v_h\|_0.$$

On the other hand, (3.7) implies

$$|I_2| \lesssim h \|u\|_6 \|DG_h^2 v_h\|_0.$$

In a conclusion, we obtain that

$$|a_h(u_h - u_I, v_h)| \lesssim h \|u\|_6 \|DG_h^2 v_h\|_0, \forall v_h \in V_h^0.$$

Choosing $v_h = u_h - u_I$ in the above estimate, we have (3.9).

The estimate (3.10) is a direct consequence of (3.9) and (3.3), together with the triangle inequality. \square

3.2. H^1 error estimate. In this section, we use the Aubin-Nitsche technique to estimate the H^1 norm error $\|\nabla u - G_h u_h\|_0$. To this end, we construct the following auxiliary problems :

1) Find $U \in H_0^3(\Omega)$ such that

$$\int_{\Omega} D^3 U : D^3 v = (G_h(u_h - u_I), \nabla v), \forall v \in H_0^3(\Omega). \quad (3.14)$$

2) Find $U_h \in V_h^0$ such that

$$a_h(U_h, v_h) = (G_h(u_h - u_I), \nabla v_h), \forall v_h \in V_h^0. \quad (3.15)$$

It is easy to deduce from (3.14) that

$$\|U\|_5 \lesssim \|G_h(u_h - u_I)\|_0, \quad (3.16)$$

and from (3.15),(3.5) that

$$\|D(G_h^2 U_h)\|_0 \lesssim \|G_h(u_h - u_I)\|_0. \quad (3.17)$$

THEOREM 3.2. *Let u_h be the solution of (2.1) and $u \in H^6$ the solution of (1.3). If the mesh \mathcal{T}_h is translation invariant, and G_h is properly defined such that (3.1)-(3.7) hold, then*

$$\|G_h(u_h - u_I)\|_0 \lesssim h^{\frac{3}{2}} \|u\|_6. \quad (3.18)$$

Consequently,

$$\|\nabla u - G_h u_h\|_0 \lesssim h^{\frac{3}{2}} \|u\|_6. \quad (3.19)$$

Proof. First, by the definition of the auxiliary problems, we have

$$\begin{aligned} (G_h(u_h - u_I), \nabla(u_h - u_I)) &= a_h(U_h, u_h - u_I) \\ &= a_h(u_h - u_I, U_h) \\ &= (f, U_h) - a_h(u_I, U_h) \\ &= (-\Delta^3 u, U_h) - a_h(u_I, U_h). \end{aligned}$$

Using the same splitting techniques in the previous theorem, we can write

$$(G_h(u_h - u_I), \nabla(u_h - u_I)) = J_1 + J_2 + J_3 + J_4,$$

where

$$\begin{aligned} J_1 &= (\nabla(\Delta^2 u), \nabla U_h - G_h U_h), \\ J_2 &= (D^2(\Delta u), G_h^2 U_h - DG_h U_h), \\ J_3 &= (D^3 u - DG_h^2 u_I, D^3 U), \\ J_4 &= (D^3 u - DG_h^2 u_I, DG_h^2 U_h - D^3 U). \end{aligned}$$

We first estimate J_1 and J_3 . By (3.7),

$$\begin{aligned} |J_1| &\lesssim h^2 \|u\|_6 \|DG_h U_h\|_0 \\ &\lesssim h^2 \|u\|_6 \|DG_h^2 U_h\|_0 \\ &\lesssim h^2 \|u\|_6 \|G_h(u_h - u_I)\|_0. \end{aligned}$$

and

$$\begin{aligned} |J_2| &\lesssim h^2 \|u\|_6 \|DG_h^2 U_h\|_0 \\ &\lesssim h^2 \|u\|_6 \|G_h(u_h - u_I)\|_0. \end{aligned}$$

Moreover, using the integration by parts,

$$\begin{aligned} |J_3| &\leq \|D^2 u - G_h^2 u_I\|_0 \|D^4 U\|_0 \\ &\lesssim h^2 \|u\|_6 \|G_h(u_h - u_I)\|_0. \end{aligned}$$

Finally, by Cauchy-Schwartz inequality,

$$\begin{aligned} |J_4| &\lesssim h^2 \|u\|_6 \|U\|_6 \\ &\lesssim h^2 \|u\|_6 \|G_h(u_h - u_I)\|_1 \lesssim h^3 \|u\|_6^2. \end{aligned}$$

Summarizing all the above estimates, we obtain

$$(G_h(u_h - u_I), \nabla(u_h - u_I)) \lesssim h^2 \|u\|_6 \|G_h(u_h - u_I)\|_0 + h^3 \|u\|_6^2.$$

Noticing that

$$\|G_h(u_h - u_I)\|_0^2 \sim (G_h(u_h - u_I), \nabla(u_h - u_I)),$$

we arrive that

$$\|G_h(u_h - u_I)\|_0^2 \lesssim h^2 \|u\|_6 \|G_h(u_h - u_I)\|_0 + h^3 \|u\|_6^2.$$

Then the estimate (3.18) follows.

The H^1 error estimate of (3.19) is a direct consequence of (3.18) and (3.2). \square

3.3. L^2 error estimate. **THEOREM 3.3.** *Let u_h be the solution of (2.1) and $u \in H^6$ the solution of (1.3). If the mesh \mathcal{T}_h is sufficiently regular and uniform, G_h is properly defined such that (3.1)-(3.7) hold, then*

$$\|u - u_h\|_0 \lesssim h^{\frac{3}{2}} \|u\|_6. \quad (3.20)$$

Proof. By (3.5),

$$\|u_I - u_h\|_0 \lesssim \|G_h(u_I - u_h)\|_0 \lesssim h^{\frac{3}{2}} \|u\|_6.$$

Then

$$\|u - u_h\|_0 \lesssim \|u - u_I\|_0 + \|u_I - u_h\|_0 \lesssim h^{\frac{3}{2}} \|u\|_6.$$

\square

REMARK 3.2. *In the second section, we observed the convergence rates $\mathcal{O}(h^2)$ both for the errors $\|u - u_h\|_0$ and $\|\nabla u - G_h u_h\|_0$. However, we can only prove the order $\mathcal{O}(h^{\frac{3}{2}})$ from our analysis. Further analysis to the scheme is desired to prove the optimal convergence rates of $\|u - u_h\|_0$ and $\|\nabla u - G_h u_h\|_0$.*

4. Numerical Experiments. In this section, we present several numerical experiments to show the convergence rates and efficiency of our method. In all our numerical experiments, G_h is chosen as the polynomial preserving recovery operator [46]. To present our numerical results, the following notations are used :

$$\begin{aligned} De &:= \|u - u_h\|_0, & D^1 e &:= \|\nabla u - \nabla u_h\|_0, \\ D_r^1 e &:= \|\nabla u - G_h u_h\|_0, & D^2 e &:= \|D^2 u - DG_h u_h\|_0, \\ D^3 e &:= \|D^3 u - DG_h^2 u_h\|_0. \end{aligned}$$

Moreover, the convergence rates are listed with respect to the degree of freedom(Dof). Noticing $\text{Dof} \approx h^{-2}$ for a two dimensional grid, the corresponding convergent rates with respect to the mesh size h are double of what we present in the tables 3.1-3.11.

Example 1. We consider the triharmonic problem

$$\begin{cases} -\Delta^3 u = f & \text{in } \Omega = (0, 1) \times (0, 1); \\ u = \partial_{\mathbf{n}} u = \partial_{\mathbf{nn}}^2 u = 0 & \text{on } \partial\Omega, \end{cases} \quad (4.1)$$

where f is chosen to fit the exact solution $u(x_1, x_2) = x_1^3(1 - x_1)^3 x_2^3(1 - x_2)^3$.

First, we apply our scheme (2.1) on regular pattern uniform triangular mesh. The corresponding numerical results are listed in Table 4.1. It shows that numerical solution u_h converges to the exact solution u at a rate of $O(h)$ in recovered H^3 norm. Also from this table, we observe that De and $D_r^1 e$ converge at a rate of $O(h^2)$ while $D^1 e$ and $D^2 e$ converge at a rate of $O(h)$. Note that convergence rate of De and $D_r^1 e$ is better than that proved in Theorems 3.2 and 3.3.

TABLE 4.1
Numerical Results Of Example 1 On Regular Pattern Uniform Mesh

Dof	De	order	$D^1 e$	order	$D_r^1 e$	order	$D^2 e$	order	$D^3 e$	order
1089	5.61e-06	–	5.76e-05	–	2.57e-05	–	4.01e-04	–	4.46e-03	–
4225	1.54e-06	0.95	2.20e-05	0.71	7.03e-06	0.96	1.73e-04	0.62	2.06e-03	0.57
16641	3.99e-07	0.99	9.65e-06	0.60	1.83e-06	0.98	8.18e-05	0.54	9.99e-04	0.53
66049	1.01e-07	0.99	4.62e-06	0.53	4.66e-07	0.99	4.03e-05	0.51	4.93e-04	0.51

Secondly, we test our scheme on uniform triangular meshes of other patterns, including the chevron, Criss-cross, and Union-Jack patterns. Numerical data are listed in 4.2, Table 4.3, and Table 4.4, respectively. Again, we observed $O(h^2)$ for De , $O(h)$ for $D^1 e$, $O(h^2)$ for $D_r^1 e$, $O(h)$ for $D^2 e$, and $O(h)$ for $D^3 e$, the same as the regular pattern.

TABLE 4.2
Numerical Results Of Example 1 On Chevron Pattern Uniform Mesh

Dof	De	order	$D^1 e$	order	$D_r^1 e$	order	$D^2 e$	order	$D^3 e$	order
1089	4.48e-06	–	6.00e-05	–	2.02e-05	–	3.81e-04	–	4.26e-03	–
4225	1.25e-06	0.94	2.22e-05	0.73	5.65e-06	0.94	1.69e-04	0.60	2.04e-03	0.54
16641	3.24e-07	0.99	9.67e-06	0.61	1.47e-06	0.98	8.14e-05	0.53	9.97e-04	0.52
66049	8.24e-08	0.99	4.62e-06	0.54	3.75e-07	0.99	4.03e-05	0.51	4.92e-04	0.51

TABLE 4.3
Numerical Results Of Example 1 On Criss-cross Pattern Uniform Mesh

Dof	De	order	$D^1 e$	order	$D_r^1 e$	order	$D^2 e$	order	$D^3 e$	order
2113	1.50e-05	–	2.91e-03	–	3.13e-05	–	3.61e-03	–	7.21e-03	–
8321	3.83e-06	1.00	1.48e-03	0.50	8.02e-06	0.99	1.83e-03	0.50	3.62e-03	0.50
33025	9.46e-07	1.01	7.20e-04	0.52	2.02e-06	1.00	8.98e-04	0.52	1.81e-03	0.50
131585	2.39e-07	0.99	3.64e-04	0.49	5.09e-07	1.00	4.55e-04	0.49	9.07e-04	0.50

Finally, we turn to the Delaunay mesh. The first level coarse mesh is generated by EasyMesh [23] followed by three levels of regular refinement. Table 4.5 presents the convergence history for the five different errors. $O(h^2)$ and $O(h)$ convergence rates are observed for L_2 and H_1 errors. As for the L_2 error of recovered gradient, $O(h^2)$ superconvergence is observed. Regarding recovered H_2 and H_3 errors, $O(h)$ convergence are observed.

In summary, we see that our method converges with optimal rates on all four tested uniform meshes as well as the Delaunay mesh.

TABLE 4.4
Numerical Results Of Example 1 On Unionjack Pattern Uniform Mesh

Dof	De	order	D^1e	order	D_r^1e	order	D^2e	order	D^3e	order
1089	2.61e-05	–	3.24e-03	–	6.30e-05	–	4.33e-03	–	9.40e-03	–
4225	6.53e-06	1.02	1.61e-03	0.51	1.59e-05	1.02	2.12e-03	0.53	4.52e-03	0.54
16641	1.63e-06	1.01	8.03e-04	0.51	4.00e-06	1.01	1.06e-03	0.51	2.22e-03	0.52
66049	4.08e-07	1.01	4.01e-04	0.50	1.00e-06	1.00	5.26e-04	0.50	1.10e-03	0.51

To show the efficiency of our method, we make some numerical comparison with the cubic C^0 interior penalty method [27] on the same Delaunay meshes. Table 4.6 shows numerical results of the C^0 interior penalty method in the L_2 norm and the energy norm defined in [27]. Consisting with the theoretical result established in [27], the error in the energy norm converges linearly and the L_2 error decays at rate $O(h^2)$.

Figures 4.1 and 4.2 depict convergent rates of these two methods(i.e. our method and the C^0 interior penalty method) under the discrete H_3 (the energy) and L_2 norms. The rates are almost the same. However, to achieve the same accuracy, our algorithm uses about one-eighth degrees of freedom of the C^0 interior penalty method.

TABLE 4.5
Numerical Results of Example 1 on Delaunay Triangulation with Regular Refinement

Dof	De	order	D^1e	order	D_r^1e	order	D^2e	order	D^3e	order
513	1.08e-05	–	9.72e-05	–	4.93e-05	–	6.21e-04	–	6.34e-03	–
1969	3.02e-06	0.95	3.04e-05	0.86	1.38e-05	0.95	2.41e-04	0.70	2.90e-03	0.58
7713	7.94e-07	0.98	1.23e-05	0.66	3.65e-06	0.97	1.08e-04	0.59	1.37e-03	0.55
30529	2.03e-07	0.99	5.77e-06	0.55	9.35e-07	0.99	5.20e-05	0.53	6.67e-04	0.52

TABLE 4.6
 C^0 Interior Penalty Method for Example 1 on Delaunay Triangulation with Regular Refinement

Dof	De	order	D_h^3e	order
4369	7.75e-06	–	6.25e-03	–
17233	2.72e-06	0.76	2.92e-03	0.55
68449	7.89e-07	0.90	1.37e-03	0.55
272833	1.58e-07	1.16	6.63e-04	0.52

Example 2. In the second example, we will show that our scheme works well also for problems nonhomogeneous boundary conditions. We consider the equation

$$-\Delta^3 u = \sin(2\pi x_1) \cos(2\pi x_2), (x_1, x_2) \in [0, 1]^2$$

whose exact solution is

$$u(x_1, x_2) = \frac{1}{512\pi^6} \sin(2\pi x_1) \cos(2\pi x_2),$$

It provides nonhomogeneous boundary conditions $u|_{\partial\Omega}, \partial_{\mathbf{n}}u|_{\partial\Omega}, \partial_{\mathbf{nn}}^2u|_{\partial\Omega}$.

As in Example 1, we first test our algorithm on regular pattern uniform triangular mesh and list the numerical results in Table 4.7. Again, D^3e decays at rate $O(h)$. As expected, both De and D_r^1e converges with order $O(h^2)$. Astonishingly, both D^1e and D^2e also converge quadratically. Namely, for this example, both D^1e and D^2e superconverge.

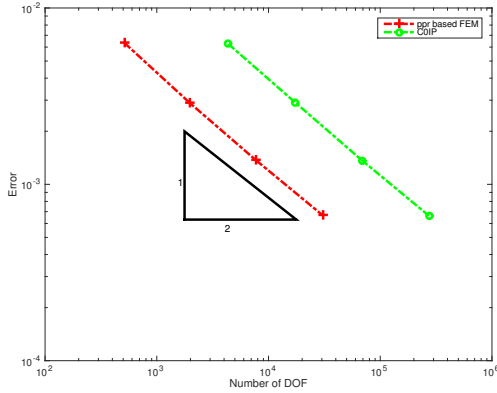


FIG. 4.1. Comparison of Discrete H_3 Errors for Example 1

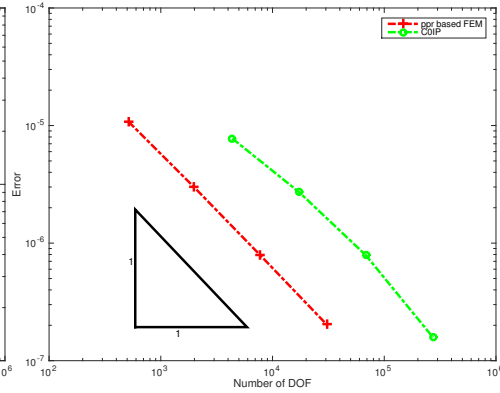


FIG. 4.2. Comparison of Discrete L_2 Errors for Example 1

TABLE 4.7
Numerical Results Of Example 2 On Regular Pattern Uniform Mesh

Dof	De	order	D^1e	order	$D^1_r e$	order	D^2e	order	D^3e	order
1089	2.50e-07	–	3.21e-05	–	1.53e-06	–	1.35e-04	–	2.25e-03	–
4225	2.66e-08	1.65	7.09e-06	1.11	1.47e-07	1.73	2.93e-05	1.13	7.65e-04	0.80
16641	3.01e-09	1.59	1.46e-06	1.15	1.92e-08	1.48	6.75e-06	1.07	3.24e-04	0.63
66049	4.75e-10	1.34	3.32e-07	1.08	3.41e-09	1.25	1.76e-06	0.98	1.37e-04	0.62

We then consider chevron pattern uniform triangular mesh. Table 4.8 clearly indicates that u_h converges to u at a rate of $O(h^2)$ under the L^2 norm, at a rate of $O(h)$ under the H^1 norm and the recovered H^2 and H^3 norms. Moreover, the recovery gradient $G_h u_h$ converges to ∇u at a rate of $O(h^2)$. We also test our algorithms on Delaunay meshes as in the previous example. The numerical data are demonstrated in Table 4.9. Similar to what we observed in Chevron pattern uniform triangular mesh, the computed error by our method converges to 0 with optimal rates under various norms.

In addition, we have tested our algorithms on other two types (Criss-cross and Union-Jack pattern) uniform triangular meshes. Since the numerical results are similar to the corresponding parts in the previous example, they are not reported here.

TABLE 4.8
Numerical Results of Example 2 on Chevron Pattern Uniform Mesh

Dof	De	order	D^1e	order	$D^1_r e$	order	D^2e	order	D^3e	order
1089	4.39e-08	–	1.08e-06	–	4.20e-07	–	1.23e-05	–	2.70e-04	–
4225	3.38e-09	1.89	4.47e-07	0.65	3.92e-08	1.75	3.65e-06	0.90	9.95e-05	0.74
16641	7.89e-10	1.06	2.22e-07	0.51	7.57e-09	1.20	1.61e-06	0.60	4.13e-05	0.64
66049	2.00e-10	1.00	1.11e-07	0.50	1.83e-09	1.03	7.84e-07	0.52	1.78e-05	0.61

Once again, we present a numerical comparison with the C^0 interior penalty method. We see from Figure 4.3 that the convergence rates of H_3 error are comparable, however, our method requires much less degrees of freedom in order to achieve the same accuracy. Figure 4.4 indicates that our method is slightly better than the C^0 interior penalty method with regard to the L_2 norm which is suboptimal. Here we

TABLE 4.9
Numerical Results of Example 2 on Delaunay Triangulation with Regular Refinement

Dof	De	order	D^1e	order	D_r^1e	order	D^2e	order	D^3e	order
513	5.52e-08	—	1.77e-06	—	3.81e-07	—	1.29e-05	—	1.44e-04	—
1969	1.17e-08	1.15	5.43e-07	0.88	8.07e-08	1.15	4.21e-06	0.83	5.78e-05	0.68
7713	2.79e-09	1.05	2.57e-07	0.55	1.97e-08	1.03	1.90e-06	0.58	1.94e-05	0.80
30529	6.86e-10	1.02	1.27e-07	0.51	4.91e-09	1.01	9.40e-07	0.51	8.52e-06	0.60

would like to point out that the error of the C^0 interior penalty method is sensitive to the penalty parameter.

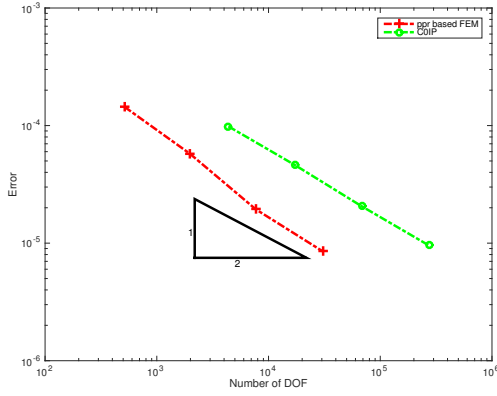


FIG. 4.3. Comparison of Discrete H_3 Errors for Example 2

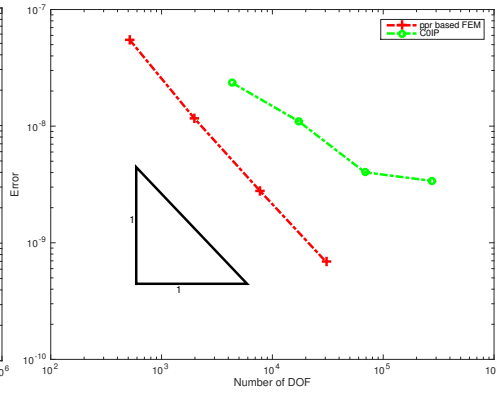


FIG. 4.4. Comparison of Discrete L_2 Errors for Example 2

Example 3. In previous two examples, we consider sixth order elliptic equations on the unit square. To show the ability of dealing arbitrary complex domain, we consider the following sixth order partial differential equation

$$-\Delta^3 u = 8e^{x_1+x_2}.$$

on the unit disk, i.e. $\Omega = \{(x_1, x_2) \in \mathbb{R}^2 : x_1^2 + x_2^2 \leq 1\}$. The exact solution is

$$u(x_1, x_2) = e^{x_1+x_2}.$$

and the corresponding boundary conditions are given by the exact solution. The initial mesh is generated by DistMesh [36] as shown in Figure 4.5. The other seven level meshes are obtained by refining the initial mesh using regular refinement. The numerical results are reported in Table 4.10. As in two previous examples, $O(h)$ convergence for D^3e , D^2e , and D^1e are observed and $O(h^2)$ convergence order are observed for De and D_r^1e .

Example 4. As in [28], we consider the following triharmonic equation

$$-\Delta^3 u = 0.$$

on the L-shaped domain $[-1, 1]^2 \setminus ([0, 1] \times [-1, 0])$ with boundary conditions such that the problem has the exact solution

$$u(x_1, x_2) = x_1^6 - x_2^6.$$

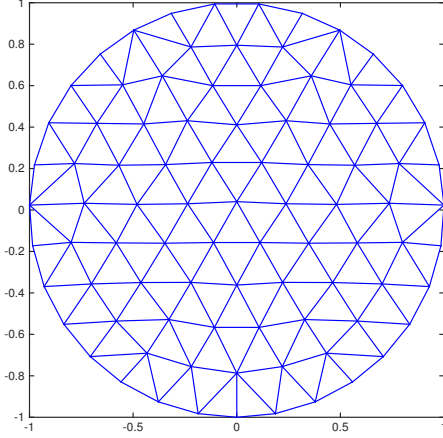


FIG. 4.5. Initial Mesh On The Unit Disk

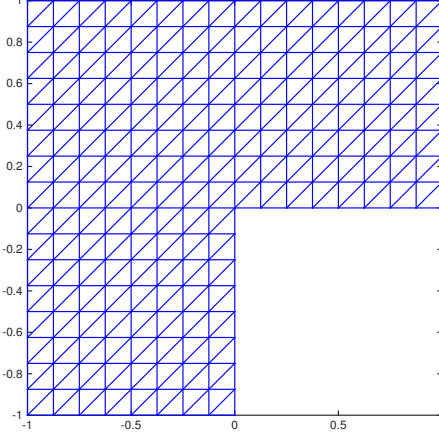


FIG. 4.6. Initial Mesh On The Lshape Domain

TABLE 4.10
Numerical Results of Sixth Order PDE in the Unit Disk

Dof	De	order	D^1e	order	D_r^1e	order	D^2e	order	D^3e	order
88	3.69e-02	–	4.76e-01	–	1.38e-01	–	1.01e+00	–	3.70e+00	–
318	1.44e-02	0.73	1.91e-01	0.71	3.21e-02	1.14	3.48e-01	0.83	1.92e+00	0.51
1207	1.84e-03	1.54	8.05e-02	0.65	4.76e-03	1.43	1.06e-01	0.89	7.14e-01	0.74
4701	4.16e-04	1.09	4.00e-02	0.51	1.20e-03	1.01	4.94e-02	0.56	3.66e-01	0.49
18553	1.04e-04	1.01	2.00e-02	0.51	3.03e-04	1.00	2.40e-02	0.52	1.99e-01	0.44
73713	2.60e-05	1.00	1.00e-02	0.50	7.57e-05	1.01	1.19e-02	0.51	9.70e-02	0.52
293857	7.01e-06	0.95	5.00e-03	0.50	1.85e-05	1.02	5.94e-03	0.50	4.62e-02	0.54

Here we use uniform meshes. The initial mesh is plotted in Figure 4.6, while our numerical results are listed in Table 4.11. As pointed out in [28], the solution u varies fast near the boundary. Even in that case, we observe the optimal convergence rates under all the norms.

TABLE 4.11
Numerical Results For Triharmonic Equation On LShape Domain

Dof	De	order	D^1e	order	D_r^1e	order	D^2e	order	D^3e	order
225	2.04e-01	–	5.78e+00	–	8.10e-01	–	1.42e+01	–	7.58e+01	–
833	2.63e-02	1.56	1.69e+00	0.94	1.24e-01	1.43	4.12e+00	0.95	2.96e+01	0.72
3201	3.54e-03	1.49	4.20e-01	1.03	2.70e-02	1.14	1.42e+00	0.79	1.35e+01	0.58
12545	6.66e-04	1.22	1.39e-01	0.81	6.67e-03	1.02	5.71e-01	0.66	6.70e+00	0.52
49665	1.44e-04	1.12	5.95e-02	0.62	1.71e-03	0.99	2.62e-01	0.57	3.35e+00	0.50
197633	3.35e-05	1.05	2.82e-02	0.54	4.55e-04	0.96	1.27e-01	0.52	1.68e+00	0.50

In summary, our numerical experiments discover that our algorithm converges with optimal rates under various norms, for sixth order equations on different kinds of domains, with homogenous or nonhomogeneous boundary conditions. In addition, comparing to some existed algorithm such as C^0 interior penalty method, our algorithm has much lower computational cost.

5. Concluding remarks. In this work, we developed a PPR based discretization algorithm for a sixth-order PDE. The algorithm has a simple form and is easy to implement. Moreover, it has optimal convergence rates as the existing conforming

and nonconforming FEMs in the literatures for sixth-order PDEs. However, the new method seems to be more advantageous with respect to computational complexity.

Generally speaking, the recovery operator is a special difference operator on nonuniform grids. It can be used to *compute* high order derivatives of a function which are piecewise polynomials but only globally in C^0 and thus can be used to discretize PDEs of higher order. On the other hand, how to choose different recovery operators for different PDEs deserves more in-depth mathematical study. Further investigation is called for to find simple and efficient algorithms for complicated PDEs.

REFERENCES

- [1] A. Adini and R.W. Clough, Analysis of plate bending by the finite element method, *NSF report G. 7337*, 1961.
- [2] M. Ainsworth J.T. Oden, *A Posteriori Error Estimation in Finite Element Analysis*, Wiley Interscience, New York, 2000.
- [3] I. Babuska and T. Strouboulis, *The Finite Element Method and Its Reliability*, Oxford University Press, London, 2001.
- [4] R. E. Bank and A. Weiser, Some a posteriori error estimators for elliptic partial differential equations. *Math. comp.*, 44(1985), 283-301.
- [5] R. E. Bank and J. Xu, Asymptotically exact a posteriori error estimators, Part I: Grid with superconvergence, *SIAM J. Numer. Anal.*, 41(2003), 2294-2312.
- [6] G. A. Baker, Finite element methods for elliptic equations using nonconforming elements, *Math. Comp.*, 31(1977), 45-59.
- [7] R. E. Bank and J. Xu, Asymptotically exact a posteriori error estimators, Part II: General unstructured grids, *SIAM J. Numer. Anal.*, 41(2003), 2313-2332.
- [8] R. Backofen, A. Rätz, and A. Voigt, Nucleation and growth by a phase crystal (PFC) model, *Phil. Mag. Lett.*, 87(2007):813C-820.
- [9] J. W. Barrett, S. Langdon, Stephen and R. Nürnberg, Finite element approximation of a sixth order nonlinear degenerate parabolic equation, *Numer. Math.*, 96(2004), 401-434.
- [10] D. Biskamp, E. Schwarz, and J.F. Drake. Ion-controlled collisionless magnetic reconnection. *Physical Review Letters*, 75(1995):3850-3853.
- [11] D. Biskamp, E. Schwarz, A. Zeiler, A. Celani, and J.F. Drake. Electron magnetohydrodynamic turbulence. *Physics of Plasmas*, 6(1999):751-758.
- [12] S. Brenner and L. Sung, C_0 interior penalty methods for fourth order elliptic boundary value problems on polygonal domains, *J. Sci. Comput.*, 22/23(2005), 83-118.
- [13] S. Brenner and L.R. Scott, *Mathematical Theory of Finite element Methods*, 3rd edition, Springer-Verlag, New York, 2008.
- [14] J. W. Cahn, On spinodal decomposition, *Acta Metall*, 9 (1961), 795-801.
- [15] G. Caginalp and P. Fife. Higher-order phase field models and detailed anisotropy. *Physical Review B*, 34(1986):4940-4943, 1986.
- [16] A. S. Chang and W. Chen. A note on a class of higher order conformally covariant equations, *Discrete and Continuous Dynamical Systems*, 7 (2001), 275C281.
- [17] H. Chen, H. Guo, Z. Zhang, and Q. Zou, A C_0 linear finite element method for two fourth-order eigenvalue problems. *IMA J. Numer. Anal.* 37 (2017), no. 4, 2120-2138.
- [18] M. Cheng and J. A. Warren. An efficient algorithm for solving the phase field crystal model, *J. Comput. Phys.*, 227(2008):6241C6248.
- [19] P.G. Ciarlet, *The Finite Element Method for Elliptic Problems*, Studies in Mathematics and its Applications, Vol.4, North-Holland, Amsterdam, 1978.
- [20] Introduction to COMSOL Multiphysics Version 5.1, March 2015, page 46.
- [21] Françoise Chatelin, *Spectral Approximation of Linear Operators*, Computer Science and Applied Mathematics, Academic Press Inc., New York, 1983.
- [22] J.F. Drake, D. Biskamp, and A. Zeiler. Breakup of the electron current layer during 3-d collisionless magnetic reconnection. *Geophysical Research Letters*, 24(1997):2921- 2924.
- [23] B. NICENO, *EasyMesh Version 1.4: A Two-Dimensional Quality Mesh Generator*, <http://www.dinma.univ.trieste.it/nirftc/research/easymesh>.
- [24] W.I. Fushchych and Z.I. Symenoh, High-order equations of motion in quantum mechanics and galilean relativity. *Journal of Physics A: Mathematical and General*, 30(1997):131-135, 1997.
- [25] H. Guo, Z. Zhang, and R. Zhao, Hessian Recovery for Finite Element Methods, *Math. Comp.*

- 86 (2017), no. 306, 1671–1692.
- [26] H. Guo, Z. Zhang, and Q. Zou, A C^0 linear finite element method for biharmonic problems based on gradient recovery, *J. Sci. Comput.* 74 (2018), no. 3, 1397–1422.
 - [27] T. Gudi and M. Neilan, An interior penalty method for a sixth-order elliptic equation, *IMA J. Numer. Anal.*, 31 (2011), 1734–1753.
 - [28] J. Hu, and S. Zhang, The minimal conforming H_k finite element spaces on R^n rectangular grids, *Math. Comp.*, 84 (2015), 563–579.
 - [29] J.E. Hilliard and J.W. Cahn, Free energy of a non-uniform system. I. Interfacial free energy, *J. Chem. Phys.*, 28 (1958), pp. 258C267.
 - [30] J.E. Hilliard and J.W. Cahn, Free energy of a non-uniform system. III. Nucleation in a two component incompressible fluid, *J. Chem. Phys.*, 31 (1959), pp. 688C699.
 - [31] Mohamed El-Gamel and Mona Sameeh, An efficient technique for finding the eigenvalues of fourth-order Sturm-Liouville problems, *Applied Mathematics*, 3 (2012), 920–925.
 - [32] L. Morley, The triangular equilibrium problem in the solution of plate bending problems. *Aero. Quart.*, 19 (1968), 149C-169.
 - [33] A. Naga and Z. Zhang, A posteriori error estimates based on the polynomial preserving recovery, *SIAM J. Numer. Anal.*, 42-4 (2004), 1780–1800.
 - [34] A. Naga and Z. Zhang, The polynomial-preserving recovery for higher order finite element methods in 2D and 3D, *Discrete and Continuous Dynamical Systems-Series B*, 5-3 (2005), 769–798.
 - [35] A. Naga and Z. Zhang, Function value recovery and its application in eigenvalue problems, *SIAM J. Numer. Anal.*, 50 (2012), 272–286.
 - [36] P.-O. Persson and G. Strang, A simple mesh generator in Matlab, *SIAM Rev.* 46 (2004), 329–345.
 - [37] L.B. Wahlbin, Superconvergence in Galerkin finite element methods, *Lecture Notes in Mathematics*, Springer-Verlag, Berlin, 1995.
 - [38] M. Wang and J. Xu, The Morley element for fourth order elliptic equations in any dimensions. *Numer. Math.* 103 (2006), 155–169.
 - [39] S.M. Wise, J.S. Lowengrub, J.S. Kim, and W.C. Johnson. Efficient phase-field simulation of quantum dot formation in a strained heteroepitaxial film. *Superlattices and Microstructures*, 36(2004) : 293–304.
 - [40] S. M. Wise, C. Wang, and J. S. Lowengrub. An energy-stable and convergent finite difference scheme for the phase field crystal equation, *SIAM J. Numer. Anal.*, 47(2009):2269C2288.
 - [41] H. Ugail. *Partial Differential Equations for Geometric Design*, Springer, NewYork, 2011.
 - [42] E. Ventsel and T. Krauthammer. *Thin Plates & Shells: Theory, Analysis, & Applications*. CRC, 2001.
 - [43] J. Xu and Z. Zhang, Analysis of recovery type a posteriori error estimators for mildly structured grids, *Math. Comp.*, 73 (2004), 1139–1152.
 - [44] S. Zhang and Z. Zhang, Invalidity of decoupling a biharmonic equation to two Poisson equations on non-convex polygons. *Int. J. Numer. Anal. Model.* 5 (2008), 73–76.
 - [45] Z. Zhang, Recovery Techniques in Finite Element Methods, in: *Adaptive Computations: Theory and Algorithms*, eds. Tao Tang and Jinchao Xu, Mathematics Monograph Series 6, Science Publisher, 2007, pp.333-412.
 - [46] Z. Zhang and A. Naga, A new finite element gradient recovery method: superconvergence property, *SIAM J. Sci. Comput.*, 26-4 (2005), 1192–1213.
 - [47] O.C. Zienkiewicz and J.Z. Zhu, The superconvergence patch recovery and a posteriori error estimates part 1: the recovery technique, *Internat. J. Numer. Methods Engrg.*, 33 (1992), 1331–1364.